Title page

Title: Prediction of solidification behavior of biodiesel containing monoacylglycerols above the solubility limit

Authors: Latifa Seniorita, Eiji Minami, Haruo Kawamoto

Affiliations: Graduate School of Energy Science, Kyoto University, Japan

Corresponding author: Eiji Minami

Address: Graduate School of Energy Science, Kyoto University, Yoshida-honmachi, Sakyo-ku, Kyoto 606-8501, Japan

Tel/Fax: +81 (0)75 753 5713

E-mail: minami@energy.kyoto-u.ac.jp

Abstract

Monoacylglycerols (MAGs) are typical impurities in biodiesel (fatty acid methyl esters, FAMEs) and are often the cause of solid precipitation because of their high melting points. In this study, the liquidus temperature of biodiesel, below which solidification of biodiesel components can occur, was measured by differential scanning calorimetry or visual observation, and was predicted by thermodynamic models. First, the solubility limit of MAGs, defined as the total MAG content above which MAGs can solidify before FAMEs, was found to be about 0.25 wt% for coconut methyl esters and about 0.5 wt% for palm methyl esters and rapeseed methyl esters. For biodiesel containing MAGs above the solubility limit, the compound formation (CF) model showed good agreement with the experimentally determined liquidus temperatures. This thermodynamic model assumed different types of MAGs solidifying simultaneously while forming molecular compounds. However, within the range of the total MAG content of actual biodiesel (typically less than 0.7 wt%), the number of fitting parameters in the CF model was excessive. This led to the use of a simplified version of the CF model with only one parameter, which still fitted the experimental results well. One parameter value was determined for biodiesel from one feedstock, allowing the liquidus temperature of biodiesel from a known feedstock to be predicted based only on the total MAG content, even for biodiesel containing diacylglycerols in addition to MAGs.

Keywords: biodiesel, monoacylglycerol, cold flow properties, thermodynamic prediction model

1. Introduction

Solid precipitates that form in biodiesel at low temperatures can clog fuel filters. Cold flow properties, such as the cloud point and cold filter plugging point, are indices of the risk of such precipitation. Many attempts to predict the cold flow properties of biodiesel have been reported [1–5]. The cloud point is the temperature at which a liquid fuel becomes cloudy because of solid precipitates; however, given that the cloud point is measured while cooling the sample, it may be underestimated because of supercooling. In the field of thermodynamics, the liquidus temperature is defined as the temperature above which a mixture becomes fully liquid, and it is measured while heating to eliminate the supercooling effect. The liquidus temperature is a good indicator of the low-temperature fluidity of biodiesel because it represents the temperature below which solid precipitates can form.

Biodiesel is a mixture of fatty acid methyl esters (FAMEs) and some minor components, such as monoacylglycerols (MAGs), diacylglycerols (DAGs), and triacylglycerols (TAGs). Of these acylglycerols, MAGs are dominant impurities because they are the end intermediates in the three-step transesterification of plant oils. Because of the high melting points of MAGs, they are often the cause of precipitation [6] and have been reported to be the majority of precipitates from soybean and palm oil biodiesel [7,8]. MAGs affect the cold flow properties of biodiesel even at low content levels, and its influence has been the focus of much attention and studied in recent years [9-12].

In high-purity biodiesel containing almost no MAGs, saturated FAMEs such as methyl palmitate solidify because of relatively high melting points. However, when the MAG content exceeds a certain limit, MAGs tend to solidify before the saturated FAMEs, significantly increasing the liquidus temperature [13]. This limit, referred to as the solubility limit in this study, has been reported to be about 0.2–0.3 wt% for saturated MAGs in biodiesel [14]. The presence of 0.2 wt% MAGs increased the cloud point and cold filter plugging point of soybean-derived biodiesel by about 5°C and 6°C, respectively [15].

48 Polymorphism of MAGs also affects the precipitation behavior. MAGs have several
49 crystal forms, termed α-, β'-, and β-types. In general, when a melt of MAG is cooled, metastable
50 α-type crystals form first, which irreversibly transition to the more stable β'-type and then β-type
51 after certain transition times [16]. Upon cooling MAG dissolved in a solvent, β'- or β-type
52 crystals can form directly [17]. The more stable crystalline form has a higher melting point,
53 increasing in the order of α, β', and β [16,17], and this fact makes the cold flow properties of
54 biodiesel more complex. Chupka et al. [14] and Girry et al. [18] have indicated the importance
55 of the MAG polymorphism on the cold flow properties of biodiesel. Therefore, our previous
56 studies have investigated the solidification behaviors of simple model mixtures (mainly binary
57 systems) that simulate biodiesel, focusing on the effect of MAGs [13,19].
58 In mixtures of FAMEs and MAGs, we found that MAGs had high activity coefficients
59 because of their two hydroxyl groups and were prone to precipitation from FAMEs [13,20]. The
60 liquidus temperatures of mixtures of FAMEs containing no or one type of MAG could be
61 predicted accurately by the non-solid-solution (NSS) model, a thermodynamic model based on
62 the hypothesis that one solid phase consists of a single substance [13,21]. However, for mixtures
63 containing two types of MAGs, the liquidus temperature deviated from the NSS model. This
64 deviation was attributed to the different types of MAGs forming molecular compounds and
65 solidifying. In such cases, the compound formation (CF) model fitted well with the
66 experimentally determined liquidus temperature [19]. Because actual biodiesel contains several
67 types of MAGs, the CF model is expected to work properly instead of the NSS model.
68 Therefore, this study aimed to demonstrate the CF model for actual biodiesel samples
69 containing MAGs in various concentrations. The liquidus temperature was determined by
70 differential scanning calorimetry (DSC) or visual observation. The performance of the CF
71 model in predicting the liquidus temperature was compared with the NSS model.
72

2. Materials and methods

2.1 Materials

Actual biodiesel samples were prepared from refined coconut, palm, and rapeseed oils, purchased from Nacalai Tesque (Kyoto, Japan), by an alkaline-catalyzed method [22]. For the reaction, methanol (>99%), sodium hydroxide (>97%), and *n*-hexane (>95%) from Nacalai Tesque were used. Approximately 100 g of oil was dissolved in 50 mL *n*-hexane, and a designated amount of 0.35 mol/L sodium hydroxide methanol solution was added. The reaction was conducted while stirring with a magnetic stirrer in a reflux reactor at the boiling point of *n*-hexane (69 °C) for 1h. The resulting mixture was purified by washing with water, dehydration with a sodium sulfate (>98.5%, Nacalai Tesque) column, and vacuum distillation. From each feedstock, three biodiesel samples with different acylglycerol contents were prepared under different reaction conditions (methanol/oil molar ratio from 3 to 9, stirring speed from 200 to 300 rpm), as summarized in Table 1. The fatty acid composition of each feedstock, as determined from the FAME content, is shown in Table 2.

High-purity FAMEs, MAGs, and DAGs shown in Table 3 were purchased and blended to prepare biodiesel surrogates to study the wide range of acylglycerol contents beyond the actual biodiesel samples. As shown in Table 4, the mixtures of FAMEs and MAGs were prepared separately to simulate the fatty acid compositions of plant oils in Table 2. However, because of the commercial unavailability of high-purity reagents, the fractions of FAME8:0 and FAME18:3 were incorporated into FAME10:0 and FAME18:2, respectively. MAG8:0 and unsaturated MAGs were also replaced with MAG10:0 and MAG18:1, respectively. These substitutions were not expected to affect the solidification behavior because the melting points of these substances are much lower than the others. The FAMEs and MAGs mixtures were then combined in various ratios to prepare biodiesel surrogates with various MAG contents. The mixture of DAGs was prepared only for palm methyl ester (PME) surrogates and mixed with the mixtures of FAMEs and MAGs to investigate the effect of DAGs.

99

100 2.2 Analytical methods

101 DSC analysis was performed (DSC-60, Shimadzu, Kyoto, Japan) to determine the
102 liquidus temperature. Approximately 10 mg of the sample was placed in an open aluminum pan
103 and exposed to dry nitrogen flow (50 mL/min). The sample was heated 20 °C above the highest
104 melting point among the sample's components to be completely melted and held for 3 min.
105 Three different conditions were then applied as follows:

106 *Condition 1*: The melted sample was cooled until the end of the first exothermic peak,
107 which means that the solid phase had formed, then reheated immediately, and the DSC profile
108 was recorded.

109 *Condition 2*: The melted sample was cooled 20 °C below the last exothermic peak to be
110 fully solidified, then reheated to record the DSC profile.

111 *Condition 3*: The melted sample in the open aluminum pan was cooled outside the DSC
112 device until the formation of precipitates was visually observed and stored at room temperature
113 for 24 h. The sample was then placed in the DSC device, cooled 20 °C below the last
114 exothermic peak as in Condition 2, and reheated to record the DSC profile.

115 These conditions were conscious of the transition of MAG polymorphs, and the
116 difference will be discussed later. The heating and cooling rates were ± 10 °C/min. The liquidus
117 temperature was determined from the peak top temperature of the highest endothermic peak in
118 the DSC profile [23].

119 For the samples with low MAG content (about 1 wt% or less), the liquidus temperature
120 was determined by visual observation, as detailed in our previous study [13], because the
121 endothermic peaks of MAGs were too weak to determine the liquidus by DSC. Approximately 6
122 g of the sample was placed in a glass cell apparatus with a magnetic stirrer and wholly melted at
123 100 °C. This relatively large amount of sample was to ensure the reliability of the observation of
124 MAG at low concentrations. Using a heat medium jacket covering the glass cell, the sample was

slowly cooled (−1 °C/min) with agitation until the first solid precipitated and held at that temperature for 5 min. It was then slowly reheated (1 °C/min) with agitation, and the temperature at which the solid completely disappeared was determined as the liquidus temperature. The sample was irradiated with laser light from a laser pointer to aid the observation, and the presence of fine solid particles was confirmed by scattered light. The DSC analysis and visual observation were repeated three times for each sample and condition, and the mean values were reported.

Gas chromatography (GC, GC-2014, Shimadzu) and high-performance liquid chromatography (HPLC, Prominence, Shimadzu) were performed to determine FAMEs and acylglycerols contents in biodiesel samples under the following conditions: GC; column, Select Biodiesel (Agilent, Santa Clara, CA, USA); oven temperature, 50 °C (1-min hold), heat to 180 °C (15 °C/min), heat to 230 °C (7 °C/min), heat to 380 °C (10 °C/min, 5-min hold); carrier gas, helium; detector, flame ionization. HPLC; column, Cadenza CD-C18 (Imtakt, Kyoto, Japan); oven temperature, 40 °C; eluent, methanol (1 mL/min); detector, refractive index.

X-ray diffraction analysis (XRD, RINT-2200-V, Rigaku, Tokyo, Japan) was performed to identify the crystal form of the solidified sample prepared by the same method as in Condition 3. Approximately 200 mg of the surrogate with 50 wt% MAG content was fully melted in a glass vial and cooled until crystals formed. After 24 h at room temperature, the crystals were collected by washing with *n*-hexane (>95%, Nacalai Tesque) on a suction filter and subjected to XRD analysis.

2.3 Thermodynamic models

Two thermodynamic models, namely the non-solid-solution (NSS) and compound formation (CF) models, were used to calculate the liquidus temperature. Detailed applications of these models were demonstrated previously [19] and explained in the supplementary material. First, Eq. 1 is derived from the theory of solid−liquid equilibrium [24]:

$$\frac{{\gamma_i}^{\mathrm{L}} x_i}{{\gamma_i}^{\mathrm{S}} z_i} = \exp\left[\frac{\Delta H_{m,i}}{R T_{m,i}}\left(\frac{T - T_{m,i}}{T}\right)\right] \quad (1)$$

where x_i and z_i are the liquid and solid mole fractions of component i, respectively, ${\gamma_i}^{\mathrm{L}}$ and ${\gamma_i}^{\mathrm{S}}$ are activity coefficients of component i in liquid and solid phases, representing deviations from the ideal liquid and solid solutions, respectively. Equation 1 can calculate the solid–liquid equilibrium temperature of the mixture from the melting point ($T_{m,i}$) and enthalpy of fusion ($\Delta H_{m,i}$) of each component i. The NSS model assumes that one solid phase consists of one component, meaning that different components are immiscible in a solid phase and solidify independently. On this assumption, because the solid phase fraction $z_i = 1$ (and thus ${\gamma_i}^{\mathrm{S}} = 1$), Eq. 1 is modified as follows:

$$T = \frac{T_{m,i}}{1 - \frac{R T_{m,i}}{\Delta H_{m,i}} \ln({\gamma_i}^{L} x_i)} \quad (2)$$

where the liquidus temperature (T) is expressed as a function of x_i. Equation 2 gives a T value for each component i, and the highest one among the components is the liquidus temperature of the mixture, at which the corresponding component i solidifies. Our previous studies revealed that binary mixtures of FAME/FAME [21] and MAG/FAME [13] followed this NSS model.

However, binary mixtures of MAG/MAG showed more complex behaviors and fitted with the CF model [19], suggesting the formation of molecular compounds. When v_1 moles of component C_1 and v_2 moles of C_2 in liquid phase produce one mole of solid compound C_{S}, this reaction is expressed as Eq. 3.

$$v_1 C_1(\mathrm{L}) + v_2 C_2(\mathrm{L}) \leftrightarrow C_{\mathrm{S}}(\mathrm{S}) \quad (3)$$

Considering the relationship between the reaction equilibrium constant and the Gibbs-Helmholtz equation for this reaction, the following CF model can be obtained [19]:

$$({\gamma_1}^{L} x_1)^{v_1} ({\gamma_2}^{L} x_2)^{v_2} = K_{\mathrm{ref}} \exp\left[\frac{\Delta H_{\mathrm{ref}}}{R T_{\mathrm{ref}}}\left(\frac{T - T_{\mathrm{ref}}}{T}\right)\right] \quad (4)$$

where K_{ref} and ΔH_{ref} are the reaction equilibrium constant and reaction enthalpy at an arbitrarily chosen reference temperature T_{ref}. The ΔH_{ref} was substituted by the weighted average of enthalpies of fusion of two components as follows.

$$\Delta H_{\mathrm{ref}} = \frac{v_1 \Delta H_{m,1} + v_2 \Delta H_{m,2}}{v_1 + v_2} \quad (5)$$

In this model, v_1 and v_2 were used as fitting parameters and determined by the least-squares method. The highest experimental liquidus temperature in the fitting region was chosen as T_{ref}. When three or more components form the molecular compound, the left side of Eq. 4 becomes $\prod(\gamma_i{}^L x_i)^{v_i}$. However, this study assumed that two MAGs having the first and second highest T in Eq. 2 produce the molecular compound. Although such a hypothesis may not necessarily reflect the real world, this study focused on demonstrating whether the form of Eq. 4 can represent the experimental results.

The $T_{m,i}$ and $\Delta H_{m,i}$ of each pure component used in the calculations are summarized in Table S1 in the supplementary information; these were measured in previous studies [13,20]. The $\gamma_i{}^L$ was estimated based on the type and number of functional groups of the components, using a modified version of the universal quasi-chemical functional group activity coefficient method, known as the UNIFAC (Dortmund) [25], which worked well in our previous studies [13,20]. All calculations were performed using algorithms coded in Microsoft Visual Basic for Excel (Microsoft, Redmond, WA, USA).

The performance of the thermodynamic models was evaluated by comparing the root-mean-square deviation (RMSD) between predicted ($T_{\mathrm{p},i}$) and experimentally determined ($T_{\mathrm{e},i}$) liquidus temperatures, defined as follows:

$$\mathrm{RMSD} = \sqrt{\frac{\sum_i^n \left(T_{\mathrm{p},i} - T_{\mathrm{e},i}\right)^2}{n}} \quad (6)$$

where the subscript i means i-th data and n is the number of data.

3. Results and discussion

3.1 Biodiesel surrogates

Figure 1 shows the liquidus temperatures determined by DSC for biodiesel surrogates (mixtures of FAMEs and MAGs) that simulated coconut, palm, and rapeseed oil methyl esters (CME, PME, and RME surrogates, respectively) as the total MAG content was varied up to 100 wt%. Such high MAG contents are far from actual biodiesel, but this experiment was conducted to study the behavior of MAGs extensively as fundamental research. In addition, by DSC analysis of these surrogates under different conditions, we can confirm the change in liquidus temperature due to the crystal transition of MAGs. In triplicate trials for each data point, experimental uncertainties were within −1.5 to +0.7 °C of the mean for CME, −1.2 to +0.5 °C for PME, and −1.1 to +0.8 °C for RME surrogates.

The predicted curves by the NSS model for α-, β'-, and β-type MAGs are also depicted in Figure 1. Note that these three curves are the result of the calculation in Eq. 2. Since the thermodynamic properties of MAGs (melting point, $T_{m,i}$, and enthalpy of fusion, $\Delta H_{m,i}$) depend on the crystal type, as shown in Table S1, these three different curves for α, β', and β-type crystals were produced.

The liquidus temperature was higher in the order of DSC analysis Conditions 1, 2, and 3. Condition 1 (squares, Fig. 1) was intended to measure the liquidus temperatures of α-type MAGs by preventing the crystal transition via immediate (just after the first solid phase had formed) and fast reheating (10 °C/min). Typically, since the α-type crystal is formed first when rapidly cooled (−10 °C/min), the liquidus temperature of α-type MAG is expected to be measured in Condition 1, as demonstrated in our previous study for MAG/FAME binary mixtures [13]. However, in the present study, the experimental results for Condition 1 are close to the calculated results for β'-type MAGs rather than α-type. It appears that the crystal transition of MAGs was faster in multicomponent systems used in the current study and changed to β'-type even in Condition 1, although the cause of this is unclear.

In Condition 2 (triangles, Fig. 1), the sample was cooled to be fully solidified before reheating. Furthermore, in Condition 3 (circles, Fig. 1), the sample was left at room temperature for 24 h before analysis. Thus, Conditions 2 and 3, especially the latter, were intended to give MAGs sufficient time for crystal transition. For the CME and PME surrogates, the liquidus temperature was higher in Condition 2 than in Condition 1, suggesting that the crystal transition of MAGs further progressed. However, the results in Condition 3 are almost unchanged from Condition 2 except in the regions of low MAG content of less than 10 wt%. In the RME surrogates, the liquidus temperatures in Condition 2 were almost the same as in Condition 1 but were higher in Condition 3. These results suggest that the liquidus temperature corresponding to the most stable β-type MAGs was measured by Condition 3. Note that even if the holding time at room temperature was extended to 330 h and 3600 h under Condition 3, the liquidus temperature did not change in all cases, indicating that 24 h was sufficient to obtain the β-type MAG crystals. The experimental results of Condition 3 are closest to the prediction curves for β-type MAGs.

To confirm this, XRD analysis of the crystals prepared by the same method as in Condition 3 was performed, with the results shown in Figure 2. Considering the XRD patterns of pure MAG16:0 crystals [26], the α-type crystal is characterized by strong diffraction peaks around 20–22 degrees; the β'-type shows distinct peaks at 15.5, 19.4, 21.3, 23.4, 25.3, and 27.1 degrees; the β-type shows broad peaks around 19–21 and strong signals around 22–24 degrees in addition to the above β'-type peaks. The crystals from the CME and PME surrogates present clear patterns mainly around 19–21 and 22–24 degrees, which are closest to the β-type diffraction pattern of β-type MAG16:0, although the peaks of CME crystals are broader than those of PME crystals. The reason for this broad is not apparent, but it may be because the CME has many types of MAGs. Thus, it is certain that the liquidus temperature determined by Condition 3 is attributed to β-type MAGs. However, crystals obtained from the RME surrogate were easily melted at room temperature during preparation and could not be analyzed by XRD.

Although the NSS model provided some indication, there are apparent deviations from the experimental results in Figure 1. Since MAGs were undergoing crystal transition in Conditions 1 and 2, the deviation may be affected by changes in crystal type. However, although the experimental results under Condition 3 were confirmed to be due to β-type MAGs, they did not match the NSS model calculations for β-type MAGs. The NSS model tended to underestimate the liquidus temperature of CME and overestimate PME and RME.

The deviations in the NSS model are within expectations given that our previous study suggested that the NSS model is not accurate for multicomponent mixtures containing multiple types of MAGs [13]. Therefore, the CF model was applied to the data obtained under Condition 3, as shown in Figure 3, compared with the NSS model. The experimental liquidus temperature increased sharply when the MAG content increased from 0 wt% in all cases (CME, PME, and RME surrogates). However, the liquidus temperature dropped slightly at about 10 wt% and then slowly increased with increasing MAG content. The behavior appeared different between the high and low MAG content regions. Therefore, Figure 3 shows two curves of the CF model (solid lines) that were individually fitted to each region for CME and PME surrogates. For RME, the experimental values could be roughly expressed by one curve because the difference between the low and high MAG regions was not so significant.

For fitting with the CF model, we assumed two MAGs forming the compound. We selected two MAGs with the first and second highest liquidus temperatures in Eq. 2: MAG18:0 and MAG12:0 for CME, MAG16:0 and MAG18:0 for PME, and MAG18:0 and MAG18:1 for RME surrogates, respectively.

As shown in Figure 3, the CF model was able to fit the experimental results well, and the fitting parameters, the stoichiometric composition v_1 and v_2, were determined. In the region of high MAG content, the compositions were uniquely determined as MAG18:0/MAG12:0 = 1.31/0.00 for CME, MAG16:0/MAG18:0 = 0.00/1.60 for PME, and MAG18:0/MAG18:1 = 0.94/0.04 for RME surrogates. Despite the assumption of compound formation, one MAG was

275 estimated to be almost zero, but the reason remains unclear. Although a set of v_1 and v_2 values
276 were determined by fitting for the wide range of MAG content up to 100 wt%, the composition
277 of the molecular compound may not necessarily be the same in all of this range. Actually, in the
278 low MAG regions of CME and PME, the compositions were changed to be
279 MAG18:0/MAG12:0 = 0.02/0.09 for CME, and MAG16:0/MAG18:0 = 0.50/0.82 for PME. The
280 reason why the tendency of the liquidus curve changed at about 10 wt% may be that the
281 composition of the compound had changed. However, because of the small number of
282 experimental data in the low MAG regions, these results were not unique, and there were many
283 other parameters to fit. The stoichiometric numbers estimated here only regressed the CF model
284 to the experimental data and do not necessarily represent the actual solid phase, especially in the
285 case of the high MAG content region. However, the important point is that the experimental
286 liquidus temperature could be expressed well in the form of the CF model.

287 Despite one of the solid fractions of MAGs (v_1 or v_2) being zero, the better
288 performance of the CF model than the NSS model is due to that the T_{ref} in Eq. 4, which means
289 the melting point of the molecular compound, was chosen from an experimental value, so that
290 the resulting curve always passed through that point. In addition, another MAG was not fixed to
291 1, serving to adjust the shape of the liquidus curve. In this sense, the CF model is semi-
292 empirical, and the good agreement with the experimental results is not surprising. The RMSD of
293 the CF model was very small, about 1°C for CME, PME, and RME, as shown in Figure 5. On
294 the other hand, the NSS model underestimated the liquidus temperature of CME and
295 overestimated PME and RME, resulting in large RMSD values of 4.9°C for CME, 3.7°C for
296 PME, and 4.3°C for RME. Underestimation, overestimation, and their degree in the NSS model
297 depend on the actual liquidus temperature of the molecular compound formed, as explained in
298 detail in the supplementary material. The general trend of what combinations and compositions
299 of MAGs form the molecular compound and how high the liquidus temperature has not yet been

clarified, so it is not easy to discuss the different performances of the NSS model for CME, PME, and RME surrogates.

3.2 Effect of DAGs

As shown in Table 1, actual biodiesel may contain not only MAGs but also DAGs and TAGs. Therefore, DAGs were added to the PME surrogates to investigate the effect on the liquidus temperature. The results are shown in Figure 4, where the plots without DAGs are taken from Figure 1(b), but Condition 3 is not shown because it almost overlapped with Condition 2. The samples with DAGs were prepared by blending the MAG and DAG mixtures in Table 4 at a ratio of 4:1 (w/w) and then mixing with the FAMEs mixture in various ratios. Figure 4 shows the liquidus temperature as a function of MAG content, which appears to be on approximately the same line regardless of the presence or absence of DAGs, although samples with DAGs gave slightly lower liquidus temperatures. There is an exception where a difference of about 5 °C is observed between the presence and absence of DAGs when the MAG content is around 10 wt%, but the differences in other data are very small. Therefore, even if DAGs are present in biodiesel, they do not affect the liquidus temperature to a great extent, and it might be sufficient to consider only MAGs to predict the liquidus temperature.

In the CF model, not only MAG/MAG but also, for example, MAG/DAG or DAG/DAG may form compounds. However, our previous studies of acylglycerol binary systems showed that all combinations of acylglycerols except MAG/MAG mixtures tended to follow the NSS model [27], meaning that DAGs and TAGs do not interact with MAGs and solidify independently as pure components. In addition, MAGs are generally present in higher concentration and have slightly higher melting points than DAGs and TAGs, meaning that MAGs will generally determine the liquidus temperature of biodiesel. Therefore, it is suggested that only the compound formation of MAG/MAG should be considered to predict the liquidus temperature of biodiesel [27]. This suggestion was supported even for multicomponent systems

by the results of Figure 4, which shows no significant difference in liquidus temperature with the presence of DAG in the mixture.

3.3 Actual biodiesel samples

Figure 5 shows the liquidus temperatures determined by visual observation for actual biodiesel samples. Because of the limited ranges of MAG content of actual biodiesel samples, some data obtained from the surrogate samples were added; filled circles are the data of surrogates, and open circles are those of actual biodiesels. Note that the actual biodiesel samples contained DAGs, but the surrogates did not. The data of actual biodiesel with MAG contents not present in Table 1 were measured by mixing biodiesels with different MAG contents. In triplicate trials for each data point, experimental uncertainties were within −0.2 to +0.2 °C of the mean for CME, −0.1 to +0.1 °C for PME, and −0.1 to +0.2 °C for RME. The liquidus temperature determined by visual observation was attributed to the β-type MAGs according to our previous study [13]. This may be because slow heating and stirring in visual observation ensure crystal transitions.

For all the biodiesel samples with very low MAG content (0.25 wt% or less for CME, 0.5 wt% or less for PME and RME) in Figure 5a–c, the experimentally determined liquidus temperature was almost constant and was governed by the solidification of saturated FAME. The results of the NSS model calculations (dashed lines, Fig. 5) also showed constant liquidus temperatures, at which FAME16:0 was predicted to solidify in CME and PME, and FAME18:0 in RME. In these regions, the liquidus temperature could be predicted from the FAME composition, leading to the constant liquidus temperature regardless of the MAG content. The calculation results by the NSS model are relatively close to the measured values (exact match in CME). Therefore, as presented in our previous study [21], the NSS model will help predict the cold flow properties based on the FAME composition for biodiesel with very low MAG content.

However, when the MAG content increased, a sudden rise in the liquidus temperature

was observed, suggesting that MAG was no longer soluble in FAMEs and started to solidify. This limit is called the solubility limit of MAGs in this study and was about 0.25 wt% for CME and 0.5 wt% for PME and RME. It is noteworthy that these limits are lower than the regulation for MAG content in biodiesel standards; European standard EN14124 stipulates a MAG content of 0.7 wt% or less [28]. Paryanto et al. [29] suggested that this regulation should be tightened to 0.40–0.62 wt% to prevent technical problems in B30 blend fuels, and this current study also supports this suggestion.

Regarding the calculation results of the NSS model, the liquidus temperature was almost constant when assuming α-type MAG because the solidification of FAME occurs in this case. In the case of CME, the liquidus temperature begins to rise at a MAG content of 0.45 wt% in the calculation for β'-type and at 0.06 wt% for β-type. These calculated results by the NSS model differ significantly from the experimental data for both the solubility limit and liquidus temperature. This discrepancy is also true for PME and RME.

In contrast, the fitting curves for the CF model (solid lines in Fig. 5) match well with the experimental results. In all types of biodiesel, the MAGs with the first and second highest liquidus temperatures in Eq. 2 were MAG16:0 and MAG18:0 (but the order was different) when the MAG content was less than 1.2 wt%; the fitting results for Figure 5 were MAG16:0/MAG18:0 = 0.10/0.88 for CME, 1.00/0.61 for PME, and 0.04/2.94 for RME, respectively. However, these were not unique, and other numbers could regress the experimental results as well. The use of two variables (v_1 and v_2) in the CF model may be excessive for fitting such narrow regions. Moreover, the numerical calculations, including the activity coefficient, were very complicated and not practical.

Therefore, we tried to simplify the CF model in Eq. 4. Replacing the mole fractions of MAGs in biodiesel (x_i) with the product of the total MAG content (M, w/w) and the fatty acid composition (c_i) gives the following equation:

$$({\gamma_1}^L x_1)^{v_1}({\gamma_2}^L x_2)^{v_2} = ({\gamma_1}^L c_1)^{v_1}({\gamma_2}^L c_2)^{v_2} M^{v_1+v_2} = K_{\mathrm{ref}} \exp\left(\frac{\Delta H_{\mathrm{ref}}}{RT_{\mathrm{ref}}}\frac{T-T_{\mathrm{ref}}}{T}\right) \quad (7)$$

The activity coefficient of MAG in FAME ($\gamma_i{}^L$) varies widely in the range of MAG content from 0 to 100 wt% [20], but in the narrower range of less than about 1 wt%, the variation is insignificant and it may be regarded as constant. The fatty acid composition (c_i) is also constant for the known feedstock. In Figure 5, we assumed that MAG16:0 and MAG18:0 formed the molecular compound, so in this case, c_1 and c_2 are the compositions of palmitic and stearic acids, respectively. Incorporating these constant terms into K_{ref} and considering $v_1 + v_2$ as one parameter v results in the following simplified CF model.

$$M^v = K_{\mathrm{ref}}{}' \exp\left(\frac{\Delta H}{RT_{\mathrm{ref}}}\frac{T-T_{\mathrm{ref}}}{T}\right) \quad (8)$$

The value of $K_{\mathrm{ref}}{}'$ was determined by choosing an experimental liquidus temperature as T_{ref}. We assumed ΔH to be 70 kJ/mol, an approximate intermediate between the enthalpies of fusion of β-type MAG16:0 and MAG18:0. The experimental results in Figure 5 were fitted using Eq. 8, and v was uniquely determined to be 0.70 for CME, 1.59 for PME, and 1.68 for RME. The parameter v, which is the sum of v_1 and v_2, lost its original meaning of representing the composition and served only to determine the shape of the liquidus curve; the larger v makes the steeper curve. The smaller v of CME than those of PME and RME was because CME contained short-chain MAGs with relatively low melting points, resulting in a more gradual liquidus curve. The fitting curves are not shown in Figure 5 because they completely overlapped with the results of the CF model. For the samples with MAG content above the solubility limit, the RMSD values of this simplified CF model were very small: 0.12 °C for CME, 0.66 °C for PME, and 0.31 °C for RME. In this way, the simplified CF model was sufficient to represent the experimental results, and the liquidus temperature is thought to be predicted based on the total MAG content if the feedstock is known.

Figure 5 includes both actual and surrogate biodiesel data, the former containing DAGs and the latter not. Nevertheless, the experimental data are on one curve of the CF model, suggesting that the effect of DAG is minor, as discussed in Section 3.2. Our previous paper [27]

showed that DAG tended not to form molecular compounds with MAG, suggesting that DAG does not affect the liquidus temperature of MAG.

The results by visual observation in Figure 5 correspond to the liquidus temperatures of β-type MAGs, which have the highest melting point among all crystal forms of MAGs. Therefore, the results in Figure 5 represent the most stringent criteria for the risk of biodiesel solidification. In our previous study [26], the cloud point was related to the solidification of α-type MAGs so that the measured cloud point would be lower than the results in Figure 5, but did not represent the real risk. Although this study dealt with the liquidus temperature, the form of Eq. 8 will also be helpful as a semi-empirical equation in predicting other cold flow properties such as the cloud point.

4. Conclusions

The liquidus temperatures of actual and simulated biodiesel fuels were measured and compared with those calculated by the NSS and CF models. The NSS model deviated significantly from the experimental results, while the CF model fitted well for a wide range of biodiesel samples with MAG content from the solubility limit to 100 wt%. The solubility limit of MAGs, above which β-type MAG crystals can solidify before FAMEs, was found to be about 0.25 wt% for CME and about 0.5 wt% for PME and RME.

However, within the range of MAG content in actual biodiesel (below 0.7 wt%), using two fitting parameters in the CF model was excessive. Within this range, the simplified CF model with only one fitting parameter and no consideration of the activity coefficient was sufficient for fitting. One parameter was determined for biodiesel from one feedstock, making it possible to calculate the liquidus temperature based only on the total MAG content. Even if the biodiesel contained DAGs, its effect on the liquidus temperature was limited, and even for such biodiesel, the liquidus temperature could be calculated only from the MAG content. For

biodiesel containing less MAGs than the solubility limit, the NSS model could roughly predict the liquidus temperature, at which point the solidification of FAME would occur.

This study demonstrated that the liquidus temperature of biodiesel containing MAGs above the solubility limit could be predicted based only on the total MAG content by the simplified CF model, even if the biodiesel contains DAGs. Thus, this model shows the potential to develop predictive models for other cold flow properties important for biodiesel applications, such as the cloud point and cold filter plugging point.

Acknowledgments

We thank Austin Schultz, Ph.D., from Edanz (https://jp.edanz.com/ac) for editing a draft of this manuscript.

Author contributions

Latifa Seniorita: conceptualization, methodology, investigation, formal analysis, writing—original draft; **Eiji Minami:** supervision, validation, writing—review & editing; **Haruo Kawamoto:** supervision, funding acquisition.

Conflict of interest

The authors declare that they have no known competing financial interests or personal relationships that could have appeared to influence the work reported in this paper.

References

[1] Pereira E, Meirelles AJA, Maximo GJ. Predictive models for physical properties of fats, oils, and biodiesel fuels. Fluid Phase Equilib 2020;508:112440. https://doi.org/10.1016/j.fluid.2019.112440.

[2] Dunn RO. Correlating the cloud point of biodiesel with its fatty acid methyl ester composition: Multiple regression analyses and the weighted saturation factor (wSF). Fuel 2021;300. https://doi.org/10.1016/j.fuel.2021.120820.

[3] Mostafaei M. Prediction of biodiesel fuel properties from its fatty acids composition using ANFIS approach. Fuel 2018;229:227–34. https://doi.org/10.1016/j.fuel.2018.04.148.

[4] Cunha CL, Torres AR, Luna AS. Multivariate regression models obtained from near-infrared spectroscopy data for prediction of the physical properties of biodiesel and its blends. Fuel 2020;261:116344. https://doi.org/10.1016/j.fuel.2019.116344.

[5] Mei D, Luo Y, Tan W, Yuan Y. Crystallization behavior of fatty acid methyl esters and biodiesel based on differential scanning calorimetry and thermodynamic model. Energy Sources, Part A Recover Util Environ Eff 2016;38:2312–8. https://doi.org/10.1080/15567036.2015.1039669.

[6] Chupka GM, Fouts L, McCormick RL. Effect of low-level impurities on low-temperature performance properties of biodiesel. Energy Environ Sci 2012;5:8734–42. https://doi.org/10.1039/c2ee22565d.

[7] Yu L, Lee I, Hammond EG, Johnson LA, Van Gerpen JH. The influence of trace components on the melting point of methyl soyate. J Am Oil Chem Soc 1998;75:1821–4. https://doi.org/10.1007/s11746-998-0337-8.

[8] Tang H, De Guzman RC, Salley SO, Ng KYS. Formation of insolubles in palm oil-, yellow grease-, and soybean oil-based biodiesel blends after cold soaking at 4 °C. J Am Oil Chem Soc 2008;85:1173–82. https://doi.org/10.1007/s11746-008-1303-1.

[9] Aisyah L, Wibowo CS, Bethari SA, Ufidian D, Anggarani R. Monoglyceride contents in biodiesel from various plants oil and the effect to low temperature properties. IOP Conference Series: Materials Science and Engineering 2018;316:012023. https://doi:10.1088/1757-899X/316/1/012023.

[10] Sarin A, Singh M, Singh NP. Effect of Monoglycerides, water and soap contamination on the low temperature flow properties of Pongamia biodiesel. i-Manager's J Future Eng Technol 2017;12:21-7. https://doi.org/10.26634/jfet.12.3.13433.

[11] Heiden RW, Schober S, Mittelbach M. Solubility limitations of residual steryl glucosides, saturated monoglycerides and glycerol in commercial biodiesel fuels as determinants of filter blockages. J Am Oil Chem Soc 2021:1-23. https://doi.org/10.1002/aocs.125 47.

[12] Dunn RO. Effects of minor constituents on cold flow properties and performance of biodiesel. Prog Energy Combust Sci 2009;35:481-9. https://doi.org/10.1016/j.pecs.2009.07.

[13] Yoshidomi S, Sugami Y, Minami E, Shisa N, Hayashi H, Saka S. Predicting solid-liquid equilibrium of fatty acid methyl ester and monoacylglycerol mixtures as biodiesel model fuels. J Am Oil Chem Soc 2017;94:1087–94. https://doi.org/10.1007/s11746-017-3029-4.

[14] Chupka GM, Yanowitz J, Chiu G, Alleman TL, McCormick RL. Effect of saturated monoglyceride polymorphism on low-temperature performance of biodiesel. Energy Fuels 2011;25:398–405. https://doi.org/10.1016/j.fuproc.2013.10.002.

[15] Dunn RO. Effects of monoacylglycerols on the cold flow properties of biodiesel. J Am Oil Chem Soc 2012;89:1509-20. https://doi.org/10.1007/s11746-012-2045-7.

[16] Maruyama T, Niiya I, Imamura M, Okada M, Matsumoto T, Horisawa M, et al. Study on polymorphism of monoglyceride. I. Transition of crystal modification of 1-monolaurin, 1-monomyristin, 1-monopalmitin, and 1-monostearin. J Japan Oil Chem Soc 1971;20:11–8. https://doi.org/https://doi.org/10.5650/jos1956.20.395.

[17] Lutton ES, Jackson FL. The Polymorphism of 1-Monostearin and 1-Monopalmitin. J Am

501 Chem Soc 1948;70:2445–9. https://doi.org/10.1021/ja01187a043.
502 [18] Girry IP, Paryanto I, Prakoso T, Gozan M. Effect of monopalmitic content and
503 temperature on precipitation rate in biodiesel-petroleum diesel blends. E3S Web of
504 Conferences 2018;52:00021. https://doi.org/10.1051/e3sconf/20185200021.
505 [19] Seniorita L, Minami E, Yazawa Y, Hayashi H, Saka S. Differential scanning calorimetric
506 study of solidification behavior of monoacylglycerols to investigate the cold-flow
507 properties of biodiesel. J Am Oil Chem Soc 2019;96:979–87.
508 https://doi.org/10.1002/aocs.12267.
509 [20] Seniorita L, Minami E, Kawamoto H. Solidification behavior of acylglycerols in fatty
510 acid methyl esters and effects on the cold flow properties of biodiesel. J Am Oil Chem
511 Soc 2021;98:727–35. https://doi.org/10.1002/aocs.12492.
512 [21] Imahara H, Minami E, Saka S. Thermodynamic study on cloud point of biodiesel with its
513 fatty acid composition. Fuel 2006;85:1666–70.
514 https://doi.org/10.1016/j.fuel.2006.03.003.
515 [22] Meher LC, Dharmagadda VSS, Naik SN. Optimization of alkali-catalyzed
516 transesterification of Pongamia pinnata oil for production of biodiesel. Bioresour
517 Technol 2006;97:1392–7. https://doi.org/10.1016/j.biortech.2005.07.003.
518 [23] Hohne GWH, Hemminger WF, Flammersheim H-J. Differential Scanning Calorimetry.
519 2nd ed. New York: Springer-Verlag Berlin Heidelberg; 2003.
520 https://doi.org/10.1007/978-3-662-06710-9.
521 [24] Smith JM, Van Ness HC, Abbott MM. Introduction to chemical engineering
522 thermodynamics. vol. 27. 7th ed. New York: McGraw-Hill Education; 2005.
523 https://doi.org/10.1021/ed027p584.3.
524 [25] Gmehling J, Li J, Schiller M. A modified UNIFAC model. 2. Present parameter matrix
525 and results for different thermodynamic properties. Ind Eng Chem Res 1993;32:178–93.
526 https://doi.org/10.1021/ie00013a024.

[26] Sugami Y, Yoshidomi S, Minami E, Shisa N, Hayashi H, Saka S. The effect of monoglyceride polymorphism on cold-flow properties of biodiesel model fuel. J Am Oil Chem Soc 2017;94:1095–100. https://doi.org/10.1007/s11746-017-3016-9.

[27] Seniorita L, Minami E, Kawamoto H. Solid-liquid phase behavior of binary mixtures of various partial acylglycerols by differential scanning calorimetry. Eur J Lipid Sci Technol 2021;2100092:1-9. https://doi.org/10.1002/ejlt.202100092.

[28] Committee for Standardization Automotive Fuels. Fatty acid methyl esters (FAME) for biodiesel engines - Requirements and test methods (EN14214). European Committee for Standardization CEN; 2019.

[29] Paryanto I, Prakoso T, Gozan M. Determination of the upper limit of monoglyceride content in biodiesel for B30 implementation based on the measurement of the precipitate in a Biodiesel–Petrodiesel fuel blend (BXX). Fuel 2019;258:116104. https://doi.org/10.1016/j.fuel.2019.116104.

List of figures

Figure 1. Liquidus temperature of coconut methyl esters (CME), palm methyl esters (PME), and rapeseed methyl esters (RME) surrogates measured in DSC using Condition 1 (squares), Condition 2 (triangles), or Condition 3 (circles); and predicted by the non-solid-solution (NSS) model using α-type (long dashed line), β′-type (dashed line), or β-type (solid line).

Figure 2. XRD profiles of precipitate crystals from coconut methyl esters (CME) and palm methyl esters (PME) surrogate biodiesels compared to pure 1-monopalmitin (MAG16:0) in various forms.

Figure 3. Liquidus temperature of coconut methyl esters (CME), palm methyl esters (PME), and rapeseed methyl esters (RME) surrogates determined from experiment by DSC (Condition 3, circles) and predicted values by the non-solid-solution (NSS, long dashed line) and compound formation (CF, solid line) models with root-mean-square deviations (RMSD).

Figure 4. Liquidus temperature of surrogate palm methyl esters (PME) that consisted of monoacylglycerols (MAGs) only (open symbols) or MAGs and diacylglycerols (DAGs) (solid symbols) when measured by various conditions in DSC. Note that the results for Condition 3 are not shown because almost overlapped with the results for Condition 2.

Figure 5. Liquidus temperature of coconut methyl esters (CME), palm methyl esters (PME), and rapeseed methyl esters (RME) determined from experiment by visual observation: actual biodiesel (open circles) and surrogate biodiesel (solid circles), with predicted values by the non-solid-solution (NSS) model (dashed lines) and compound formation (CF) model (solid line).

List of tables

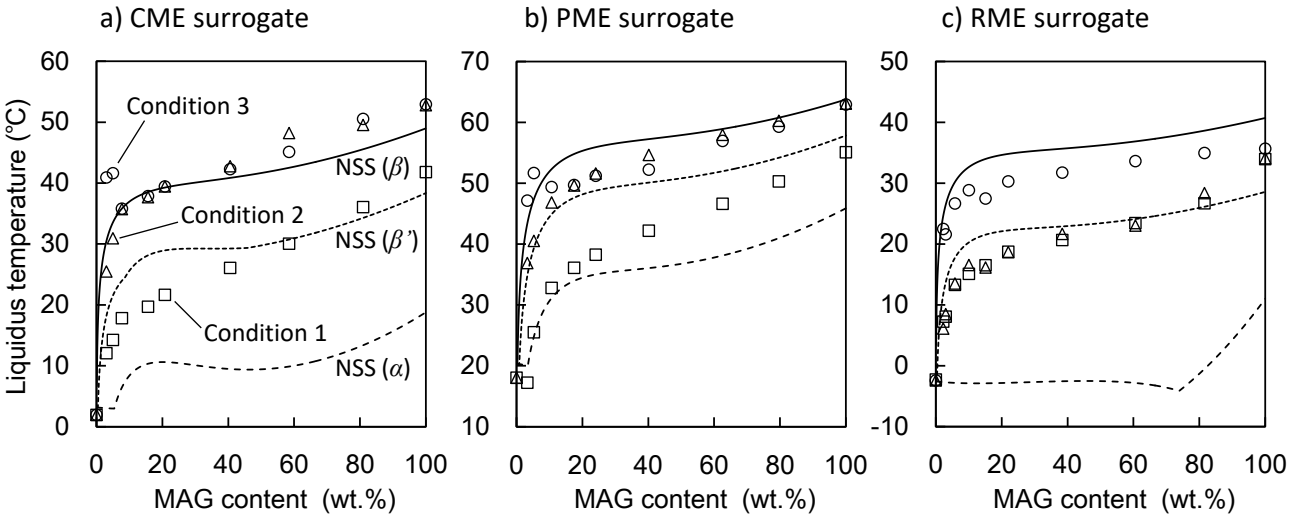

Figure 1

Seniorita, et al.

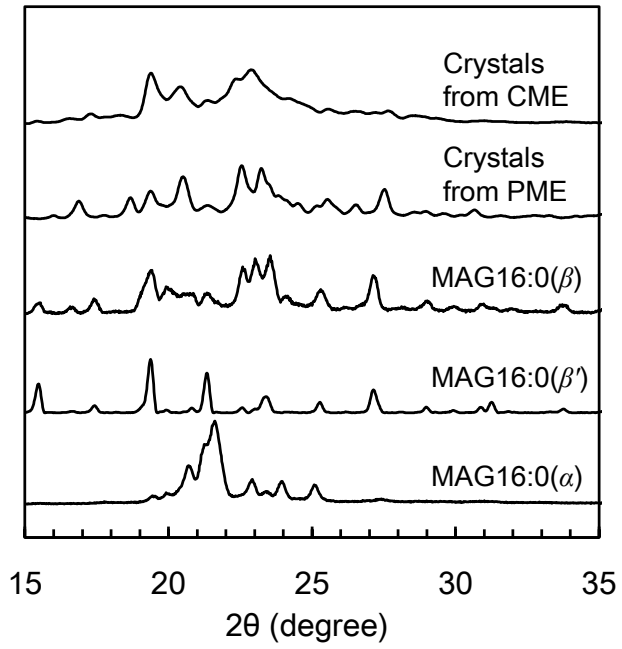

Figure 2

Seniorita, et al.

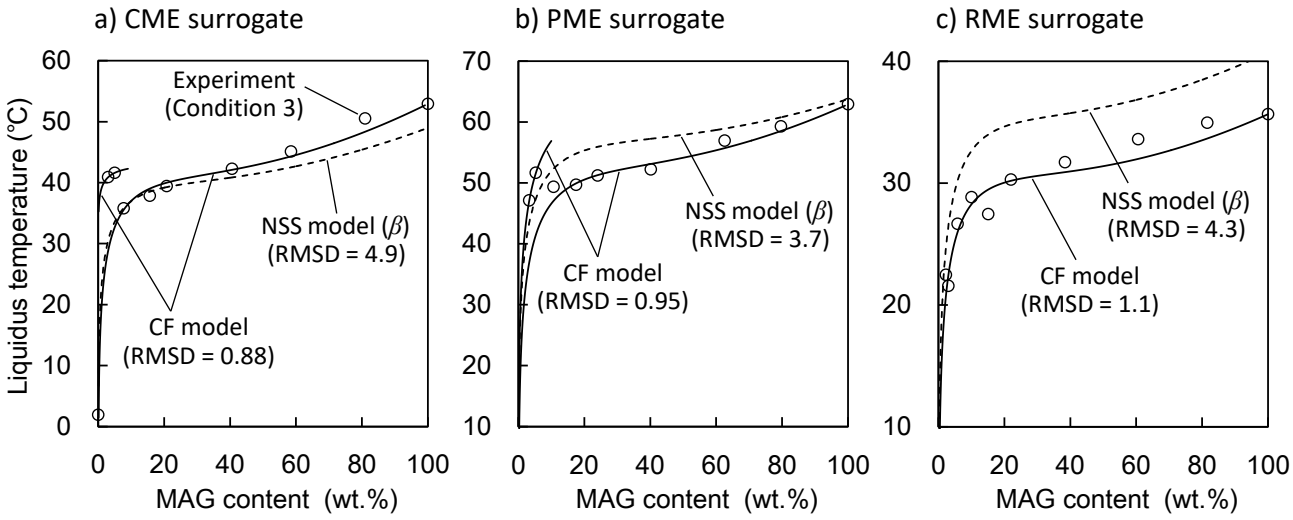

Figure 3

Seniorita, et al.

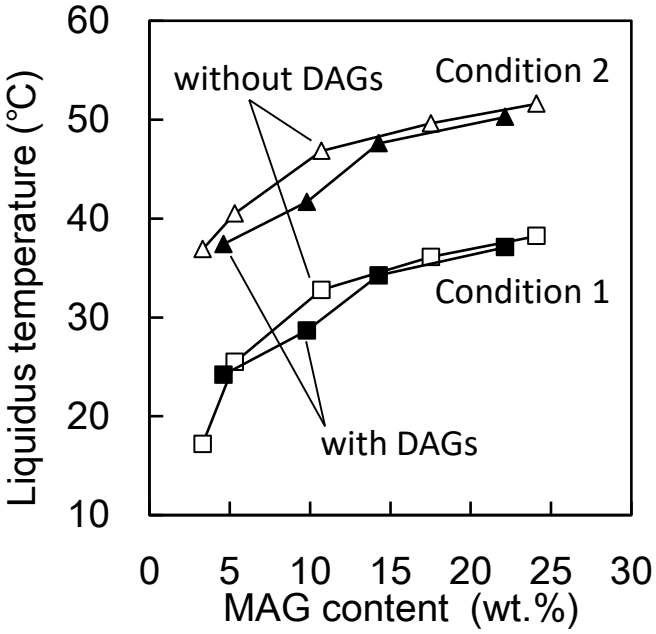

Figure 4

Seniorita, et al.

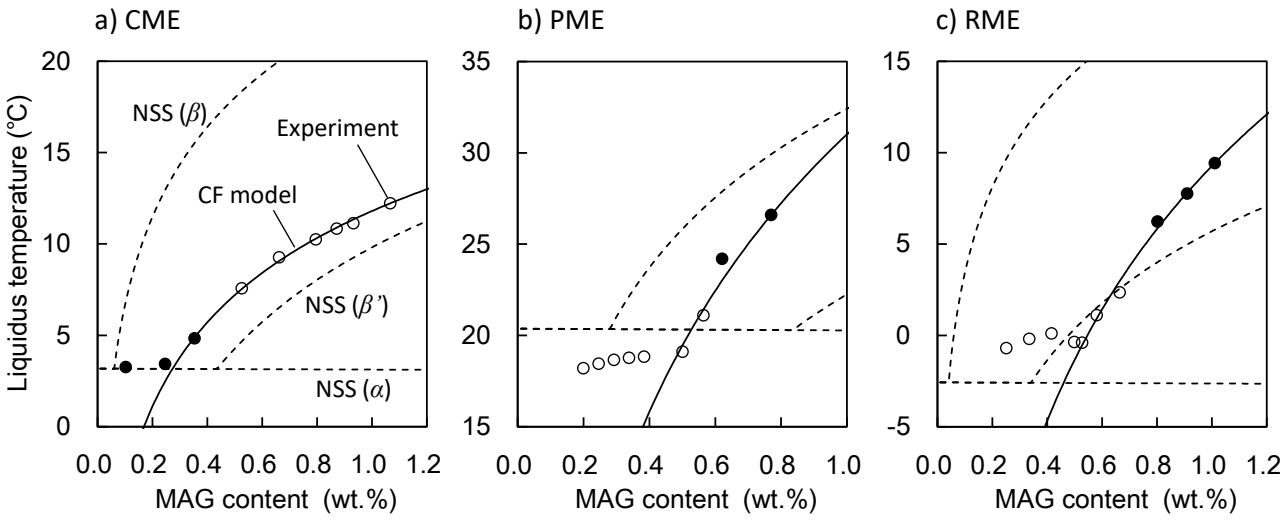

Figure 5

Seniorita, et al.

Table 1. Contents of fatty acid methyl esters (FAMEs) and acylglycerols in biodiesel samples prepared from various plant oils (wt%).

	Coconut methyl esters (CME)			Palm methyl esters (PME)			Rapeseed methyl esters (RME)		
	CME1	CME2	CME3	PME1	PME2	PME3	RME1	RME2	RME3
Total FAMEs	99.47	99.13	97.85	99.80	99.56	98.31	99.75	98.64	96.54
Total MAGs	0.53	0.87	1.20	0.20	0.43	0.56	0.25	0.53	0.66
Total DAGs	-	-	0.47	-	-	0.30	-	0.45	0.32
Total TAGs	-	-	0.47	-	-	0.83	-	0.38	2.48

MAGs, monoacylglycerols; DAGs, diacylglycerols; TAGs, triacylglycerols

Table 2. Fatty acid compositions (wt%) of biodiesel samples determined from the fatty acid methyl ester (FAME) contents.

	CME	PME	RME
Caprylic (8:0)	4.7	-	-
Capric (10:0)	4.2	-	-
Lauric (12:0)	43.9	-	-
Myristic (14:0)	19.7	0.7	-
Palmitic (16:0)	11.5	41.9	3.5
Stearic (18:0)	5.1	8.9	6.7
Oleic (18:1)	8.3	33.8	54.4
Linoleic (18:2)	1.5	13.6	21.6
Linolenic (18:3)	-	-	9.8
Others	-	0.3	2.4

CME, coconut methyl esters; PME, palm methyl esters; RME, rapeseed methyl esters

Table 3. Pure components used to prepare biodiesel surrogates.

Component	Abbreviation	Manufacturer	Purity (%)
Methyl caprate	FAME10:0	MP Biomedicals LLC, Solon, Ohio, USA	99
Methyl laurate	FAME12:0	Sigma-Aldrich Japan, Tokyo, Japan	99.5
Methyl myristate	FAME14:0		99
Methyl palmitate	FAME16:0		99
Methyl stearate	FAME18:0	Nacalai Tesque Inc., Kyoto, Japan	99.5
Methyl oleate	FAME18:1	Sigma-Aldrich Japan, Tokyo, Japan	99
Methyl linoleate	FAME18:2		99
1-Monocaprin	MAG10:0	Olbracht Serdary Research Laboratories, Toronto, Canada	99
1-Monolaurin	MAG12:0	Nu-Chek Prep, Inc., Elysian, Minnesota, USA	99
1-Monomyristin	MAG14:0	Tokyo Chemical Industry Co., Ltd., Tokyo, Japan	97
1-Monopalmitin	MAG16:0	Olbracht Serdary Research Laboratories, Toronto, Canada	99
1-Monostearin	MAG18:0		99
1-Monoolein	MAG18:1		99
1,3-Dipalmitin	DAG16:0	Olbracht Serdary Research Laboratories, Toronto, Canada	99
1,3-Distearin	DAG18:0		99
1,3-Diolein	DAG18:1	Larodan Fine Chemicals AB, Solna, Sweden	99

Table 4. Composition of FAME, MAG, and DAG mixtures (wt%) for preparing surrogate biodiesel samples that simulate the composition of CME, PME, and RME.

Fatty acid moieties	FAMEs			MAGs			DAGs
	CME	PME	RME	CME	PME	RME	PME
Caprin (10:0)	9.0	-	-	9.2	-	-	-
Laurin (12:0)	43.9	-	-	43.9	-	-	-
Myristin (14:0)	20.4	0.8	-	21.2	0.8	-	-
Palmitin (16:0)	11.5	44.0	3.5	9.2	44.1	3.5	45.4
Stearin (18:0)	5.3	8.9	2.6	6.5	8.6	2.5	7.8
Olein (18:1)	8.3	36.1	59.8	10.0	46.6	94.0	46.8
Linolein (18:2)	1.6	10.3	34.1	-	-	-	-

FAMEs, fatty acid methyl esters; MAGs, monoacylglycerols; DAGs, diacylglycerols; CME, coconut methyl esters; PME, palm methyl esters; RME, rapeseed methyl esters

Table S1. Melting point $T_{m,i}$, enthalpy of fusion $\Delta H_{m,i}$, and number of UNIFAC functional groups of each pure component.

Component	Abbreviation	Crystal type	$T_{m,i}$ (°C)	$\Delta H_{m,i}$ (kJ mol^{-1})	Number of UNIFAC functional group						
					CH_3	CH_2	CH	CH=CH	OH(p) [a]	OH(s) [b]	CH_2COO
Methyl caprate	FAME10:0 [c]	-	-14.0	27.0	2	7	-	-	-	-	1
Methyl laurate	FAME12:0 [d]	-	4.5	36.4	2	9	-	-	-	-	1
Methyl myristate	FAME14:0 [c]	-	18.1	53.0	2	11	-	-	-	-	1
Methyl palmitate	FAME16:0 [d]	-	29.8	60.4	2	13	-	-	-	-	1
Methyl stearate	FAME18:0 [e]	-	38.4	62.2	2	15	-	-	-	-	1
Methyl oleate	FAME18:1 [d]	-	-20.7	41.6	2	13	-	1	-	-	1
Methyl linoleate	FAME18:2 [d]	-	-42.4	36.2	2	11	-	2	-	-	1
1-Monocaprin	MAG10:0 [c]	α	24.3	16.9	1	9	1	-	1	1	1
		β′	44.2	23.9							
		β	54.3	41.5							
1-Monolaurin	MAG12:0 [d, f]	α	44.8	22.3	1	11	1	-	1	1	1
		β′	59.5	30.0							
		β	62.3	38.0							
1-Monomyristin	MAG14:0 [c]	α	56.7	26.9	1	13	1	-	1	1	1
		β′	67.5	39.8							
		β	68.7	50.6							
1-Monopalmitin	MAG16:0 [d]	α	66.4	34.1	1	15	1	-	1	1	1
		β′	72.7	49.8							
		β	75.7	63.6							
1-Monostearin	MAG18:0 [e]	α	74.2	39.2	1	17	1	-	1	1	1
		β′	78.0	65.7							
		β	81.6	83.5							
1-Monoolein	MAG18:1 [d, f]	α	15.0	11.0	1	15	1	1	1	1	1
		β′	30.1	30.2							
		β	35.0	49.4							

[a] Primary alcohol.

[b] Secondary alcohol.

[c] Data taken in the current study; [d] Data from Yoshidomi S, et al., J Am Oil Chem Soc, 2017, 94, 1087–1094.; [e] Data from Seniorita L, et al., J Am Oil Chem Soc, 2021, 98, 727–735.

[f] The enthalpy of β'-type MAG12:0 and MAG18:1 could not be measured because the crystal transition was too fast, so the intermediate value between α and β was used.

Supplementary explanation about the NSS and CF models

Figure S1 shows an example of the liquidus curve of a binary mixture of substances A and B. In the non-solid-solution (NSS) model (i.e., A and B do not form molecular compounds), the liquidus curve is shown by the solid lines, where pure substance A precipitates at a-c and pure B precipitates at c-e. The lines a-c and c-e are represented by the following equations, respectively, and their intersection point c is called the eutectic point.

$$T = \frac{T_A}{1-\frac{RT_A}{\Delta H_A}\ln(\gamma_A{}^L x_A)} \quad \text{(S1)}$$

$$T = \frac{T_B}{1-\frac{RT_B}{\Delta H_B}\ln(\gamma_B{}^L x_B)} \quad \text{(S2)}$$

When the mole fraction of B (x_B) is 0 (pure A), the liquidus temperature coincides with the melting point of A (T_A). When x_B = 1 (pure B), the liquidus temperature coincides with the melting point of B (T_B). When A and B solidify while forming the molecular compound A_xB_y with a specific composition *x*:*y*, the liquidus curve is shown as the dotted line b-f-d, where the vertex f means the melting point of A_xB_y. Pure component A precipitates at a-b, the compound A_xB_y precipitates at b-f-d, and pure B precipitates at d-e. In this case, the compound formation (CF) model below was applied to the region between b and d.

$$(\gamma_A{}^L x_A)^x(\gamma_B{}^L x_B)^y = K_\mathrm{ref}\exp\left[\frac{\Delta H_\mathrm{ref}}{RT_\mathrm{ref}}\left(\frac{T-T_\mathrm{ref}}{T}\right)\right] \quad \text{(S3)}$$

The melting point of the molecular compound A_xB_y ($T_{\mathrm{A}x\mathrm{B}y}$) was chosen as T_ref, and the composition *x*:*y* could be determined by least-squares fitting with the experimental results. The NSS model (Eqs. S1 and S2) is a monotonically varying function, while the CF model (Eq. S3) can represent upwardly convex liquidus curves, as shown in Figure S1. Figure S1 shows the case where the liquidus temperature by the CF model is always higher than the NSS model.

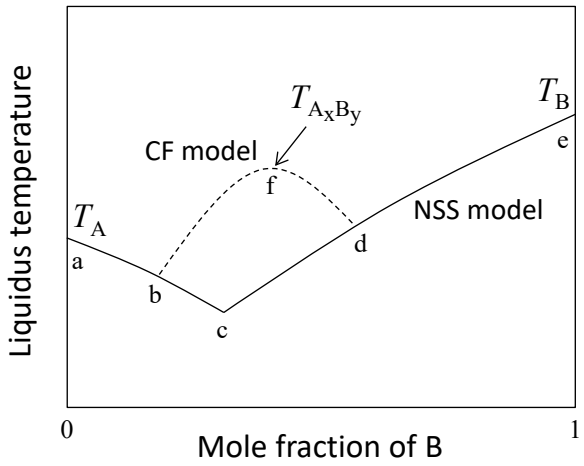

Figure S1. The case of compound formation (CF) model > non-solid-solution (NSS) model (T_A and T_B, melting points of pure A and B, respectively; T_{AxBy}, the melting point of the molecular compound A_xB_y)

On the other hand, Figure S2 shows a case where the liquidus temperature by the CF model can be lower than that by the NSS model. In this case, pure component A precipitates according to the NSS model at a-c-b, molecular compound A_xB_y precipitates according to the CF model at b-g-f-d, and pure component B precipitates at d-e. At c-b-g, the CF model shows lower liquidus temperature than the NSS model.

Thus, whether the CF model gives higher or lower values than the NSS model is complex, depending on the types of components A and B and their composition. It can only be stated that whether the NSS model overestimates or underestimates the liquidus temperature depends on the combination and composition of the components that formed the molecular compound, and no general trend can be stated.

Figures S1 and S2 are the cases where a single molecular compound A_xB_y is observed. If multiple molecular compounds, for example, $A_{x1}B_{y1}$ and $A_{x2}B_{y2}$ with different compositions, are possible, multiple upwardly convex curves may appear, as shown in Figure S3. These cases in Figures S1, S2, and S3 were the features observed in binary mixtures of monoacylglycerols (MAGs) in our previous study (Seniorita L, et al., J Am Oil Chem Soc, 2019, 96, 979–987).

The current study applied the NSS and CF models to biodiesel samples. When the NSS model was applied to a multi-component system, Eq. S4 was calculated for all components *i*.

$$T = \frac{T_i}{1-\frac{RT_i}{\Delta H_i}\ln(\gamma_i{}^L x_i)} \qquad \text{(S4)}$$

Of all the components *i*, the one with the highest liquidus temperature *T* in Eq. S4 precipitates first at that temperature. The higher melting point T_i and the larger fraction x_i give the higher *T*. Although the MAG content in biodiesel is low, it often has the highest *T* among the biodiesel components due to its very high melting point.

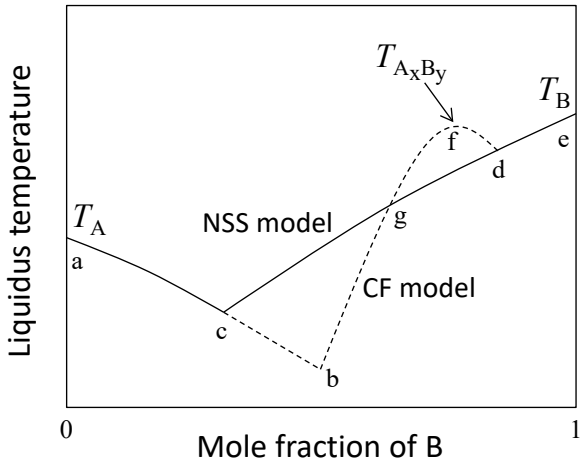

Figure S2. The case of compound formation (CF) model < non-solid-solution (NSS) model (T_A and T_B, melting points of pure A and B, respectively; T_{AxBy}, the melting point of A_xB_y)

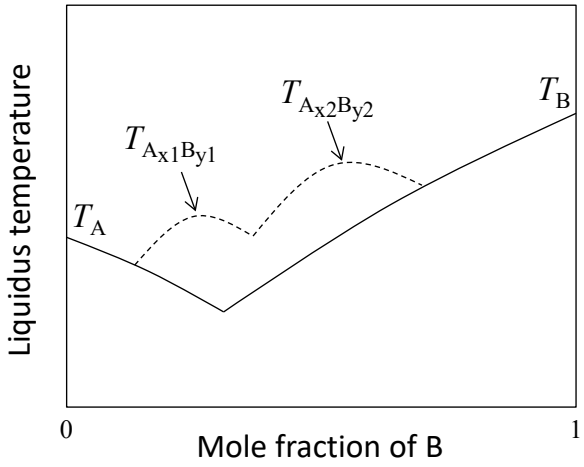

Figure S3. The case of multiple molecular compounds (T_A and T_B, melting points of pure A and B, respectively; T_{Ax1By1} and T_{Ax2By2}, melting points of $A_{x1}B_{y1}$ and $A_{x2}B_{y2}$, respectively)

The calculations by the NSS model for biodiesel with various MAG contents make a liquidus curve like the solid line in Figure S4. At the total MAG content of 100% (i.e., the mixture contains only MAGs), one of MAGs (typically 1-monopalmitin or 1-monostearin) with the highest T ($=T_{\mathrm{NSS}}$) precipitates at that temperature. The liquidus temperature decreases as the total MAG content decreases because the value of T decreases as the composition x_i of the precipitating MAG decreases. For binary mixtures of fatty acid methyl ester (FAME) and MAG, the NSS model agreed well with the experimentally determined liquidus temperature in our previous study (Yoshidomi S, et al., J Am Oil Chem Soc, 2017, 94, 1087–1094). This might be because there was only one type of MAG in the mixture, so the MAG could not form the molecular compound.

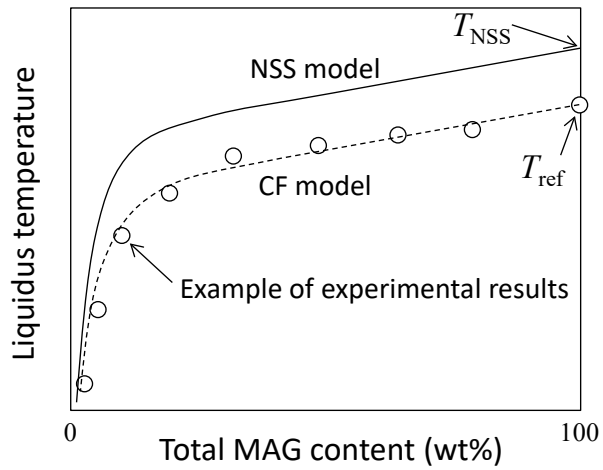

Figure S4. Fitting by the CF model, compared with the NSS model

However, as demonstrated in the current study, for biodiesel containing multiple MAGs, the experimental liquidus temperature deviated from the NSS model due to the MAGs forming molecular compounds. Whether the measured values are higher or lower than the NSS model depends on the combination and composition of the MAGs that form the molecular compounds, as explained in Figs. S1 and S2. It is difficult to discuss the general trend regarding overestimation or underestimation, and the degree of discrepancy.

In the CF model, the highest one of the experimentally determined liquidus temperatures was chosen as T_{ref}. Therefore, the liquidus curve by the CF model always passed through this point, as shown in Figure S4. Furthermore, the compositions x and y (v_1 and v_2 in the paper) of the molecular compounds were determined by least-squares fitting with other experimental results. Therefore, it is natural that the CF model matched well with the experimental results better than the NSS model that calculates the liquidus temperature only from the actual melting points and melting enthalpies of pure components in the mixture.

However, in Figure S4, the total MAG content varies widely from 0 to 100%, and the composition x:y of the molecular compound may not be necessarily constant. Therefore, the x:y determined by least-squares fitting does not necessarily reflect the actual behavior. In fact, for a wide range of total MAG content, one of x and y tended to be zero in the current and previous studies (Seniorita L, et al., J Am Oil Chem Soc,

2019, 96, 979–987). The reason why the CF model was better than the NSS model even though x or y was zero was that one of the experimental points was chosen as T_{ref}, and non-zero x or y was not fixed to 1, serving as a parameter to determine the shape of the liquidus curve.